Artículo **Revista de Tecnología e Innovación**
Septiembre 2016 Vol.3 No.8 61-69

Cathodic Current Distribution in a PEMFC for Five Different Air Flow-Field Designs

HIDALGO-PIMENTEL, Pablo*†, OROZCO-GAMBOA, Germán, GARCÍA-GARCÍA, Raúl, ZAMORA-ANTUÑANO, Marco y OLIVARES-RAMÍREZ, Juan.

Universidad Tecnológica de San Juan del Río. División de Química Industrial y Energías Renovables, Cuerpos Académico de Quìmica y Energìas Renovables. Av. La Palma no. 125, Col. Vista Hermosa, San Juan del Río, Qro. C.P. 76800
Centro de Investigación y Desarrollo Tecnológico en Electroquímica (CIDETEQ). Sanfandila; Parque Tecnológico Querétaro s/n Sanfandila, Pedro Escobedo, Qro. C.P. 76703

Recibido Julio 19, 2016; Aceptado Septiembre 13, 2016

Resumen

Se estudio mediante simulación por computadora la distribución de las corrientes eléctricas de cinco diferentes diseños de los campos de flujo del ánodo, los cuales se esperan usar en una pila de hidrógeno. El diseño 1 consiste en canales tipo serpentín con cambios abruptos de la dirección del flujo. Los diseños 2 y 3 también corresponden a una distribución serpentín, pero con cambios graduales en el flujo. El diseño 4 entrecruzado (Criss-Cross) redirecciona el flujo constantemente, mientras que el diseño 5 se basa en canales rectos y paralelos. Los diseños 1 a 3 tienen una sola entrada de flujo, mientras que los diseños 4 y 5 tienen tres. Estos dos últimos diseños muestran una distribución mas uniforme de las corrientes eléctricas que los otros diseños. Se concluye que las entradas de flujo situadas eficazmente tienen tanta importancia como la configuración de los canales. La distribución en paralelo (diseño 5) presentó el mejor desempeño.

Distribuciòn de corriente catòdca, PEMFC, Diseños de flujo de campo

Abstract

A numerical investigation was conducted to simulate electrical current distributions in five different cathode-side flow-field designs. Design 1 consisted in serpentine channels with abrupt changes in flow direction. On the other hand, Designs 2 and 3 were made of serpentine channels with a more gradual change in flow direction. Design 4 (criss-cross) was based on continually redirecting the flow, while Design 5 was made with straight parallel channels. Designs 1-3 have one intake, while designs 4 and 5 have three. The latter two produced more uniform electrical current distributions than designs 1-3. We concluded that the intakes situated effectively within each design are as important as the shape of the channel configuration. Finally, the parallel channel flow field (Design 5) is the best alternative for current collectors due to its better performance.

Cathodic current distribution, PEMFC, Air flow-field designs

Citación: HIDALGO-PIMENTEL, Pablo, OROZCO-GAMBOA, Germán, GARCÍA-GARCÍA, Raúl, ZAMORA-ANTUÑANO, Marco y OLIVARES-RAMÍREZ, Juan. Cathodic Current Distribution in a PEMFC for Five Different Air Flow-Field Designs. Revista de Tecnología e Innovación 2016, 3-8: 61-69

*Correspondencia al Autor (Correo electrónico: mazamoraa@utsjr.edu.mx)
†Investigador contribuyendo como primer autor.

Introduction

There is no consensus about the projected date of the global peak-oil production due to the lack of accurate technology to determine the stock of current world oil supplies. However, if the rate of production and consumption of the Mexican oil supplies remains unchanged, then the Mexican reserves might be depleted before 2016. Consequently, in the Mexican Energy Market it is necessary to incorporate renewable energy supplies combined with the fuel cell technology.

The essential components of a proton exchange membrane fuel cell (PEMFC) are an anodic catalyst layer, an electrolyte, a cathodic catalyst layer, and current collectors. Additionally, gaskets for preventing gas leakage between the anode and the cathode have to be considered. Current collectors, which also provide the conduits for gas distribution, are bipolar plates in a stack; they occupy over 90% of the volume and contribute 80% of the mass of a fuel cell stack. Flow fields can be effectively designed through the optimization of their configuration and shape, thus resulting in improved current collectors. This is desirable for achieving higher electrical power. Therefore, the study of various plate designs was performed by simulating the processes within a PEMFC.

Three different versions serpentine gas flow field design were investigated because it is usually the reference of choice in the literature (Li, X., & Sabir, I. 2005; Park, J., & Li, X. 2007). Our versions consisted on typical serpentine flow channel design, which has a cross section of around $1mm^2$ and the length of up to a few meters with many changes in flow direction. The fourth design consisted of a criss-cross pattern (Rivas, Hidalgo, Chapman, & Orozco, 2010).

This latter design was first proposed by Barreras *et al* (2008) and modified in our previous work (Rivas, *et al*, 2010).This design was selected for study because it reduces the blockage problem caused by the accumulation of water droplets on the cathode side, which occurs in serpentine designs. The last design consisted in parallel straight-line channels in which the flow direction remains unchanged.

The serpentine flow channel is one of the most common channel designs for PEMFC (1-2) and it was selected as reference for compared the new geometries. The goal of this study was to measure the electrical current distribution in these designs to find an efficient and a commercially viable PEMFC.

Methodology

Fluid flow and mass transfer in the gas-distribution plates were modelled numerically from a macro-scale perspective. Computational fluid dynamics (CFD) software provided by Multiphysics COMSOL® v. 3.4 was used to simulate the resulting electrical current distributions in the five flow-field designs (5). The simulation began when a flow-field channel design was drawn using the Computer Aided Design (CAD) function of this software. The geometric model consists of three regions: the gas-flow channels, a gas-diffusion layer and a cathode. In the gas diffusion layer, such as a porous carbon cloth, only diffusional processes occur, and in the cathode the electrochemical reaction takes place.

ISSN-2410-3993

The assumptions made in the fuel-cell modelling were: 1) A three-dimensional (3-D) and a single-phase model; 2) air and water vapor were considered ideal gases; 3) the flow was laminar, steady and incompressible; 4) the electrical power behavior of the cell was kinetically controlled by an oxygen reduction reaction (ORR), 5) the cathode and gas-diffusion layer were isotropic and homogeneous; 6) the ohmic potential drop in the current collector and gravity were negligible; 7) the process was isothermal, and 8) the gas phase diffuses in the x, y and z axis.

The governing transport equations used to describe the species transport within the cathode chamber of the fuel cell are listed in Table I, and their scalar equations are shown in Table II. The boundary conditions are listed in Table III and data came from the literature (5), including the molar diffusion volumes (6), the exchange current density (7) and the gas diffusion layer thickness (2). The Navier-Stokes equation (Li, 2005) was solved first in order to determine the gas velocity field in the channels. This equation was subject to boundary conditions (Guzman, Verde, Bustos, Manriquez, Terol, Arriaga, & Orozco, 2009; Jeon, Greenway, Shimpalee, & Van Zee, 2008; Boddu, Marupakula, Summers, & Majumdar, 2009). Besides, the gas species (i.e., N_2, O_2, H_2O) were taking into consideration; therefore, a multi-component diffusion (Stefan-Maxwell) equation (Park, *et al,* 2007) was needed to solve the diffusion layer. The Stefan-Maxwell equation (Park, *et al,* 2007) needs to incorporate scalar relations for fluid properties (Rivas, et al, 2010; Barreras, et al, 2008; Ab, C. 2008). Also, equation (Park, *et al,* 2007) was solved considering the convective flux equation. Meanwhile, equation (Rivas, *et al*, 2010was solved using the velocity in pore Ferng, & Lu, 2008) and mass flux vectors, and these latter equations were determined by electrode-reaction kinetics (Perry & Green, 2008).

The CFD software employs a finite-element method for solving the partial differential equations (PDE). This method involves dividing the domain of the PDEs of interest into a finite number of linear elements (i.e., "mesh"). The triangular mesh offers better conformity to curvature than the square elements, which were used mostly in areas with right angles since it reduces the number of mesh elements required. The program allows refining of the mesh, carefully adjusting the type and size of elements on any curvature of the geometry. A mesh consisting of 18000 computational elements was applied to the domain. The iterative computations were terminated once the value of the residues fell to less than $1x10^{-6}$.

A computer with a dual-core processor at a speed of 3.0 GHz and 8 GB of RAM was used. The parametric nonlinear numerical method and further details have been described extensively by Rivas (3).

The Governy Equations are:

Navier Stokes Laminar Flow

$$\rho\frac{\partial u}{\partial t}-\nabla.u\left(\nabla u+(\nabla u)^{T}\right)+\rho u.\nabla u+\nabla\rho=0 \tag{1}$$

Stefan Maxwell Diffusion and convection

$$\nabla.\left[-\rho\omega_i\sum_{j=1}^{N}D_{ij}^{eff}\frac{M}{M_j}\left(\nabla\omega_J+\omega_j\frac{\nabla M}{M}\right)+\rho\omega_i u\right]=0 \tag{2}$$

The equations are written in indicial-tensor notation with ρ, density kg/m3; t, time s; μ dynamic viscosity of oxygen = 2x10-5 Pa-s (5); u, velocity vector m/s; p, pressure Pa; ωi, weight fraction of the i species; with inlet mass fraction O2 = 0.1447, mass fraction of H2O = 0.3789 and mass fraction of N2= 0.4764; Deff,ij, effective binary diffusion coefficient, see equation (Barreras, et al , 2008); M, total molar mass of the mixture g/mol, see equation (Ab, C, 2008); Mj, molecular weight of species j, g/mol MO2, molecular weight of O2 =32 g/mol; MH2O, molecular weight of H2O = 18 g/mol; MN2, molecular weight of N2 = 28 g/mol.

The scalar equiations are:

Stefan-Maxwell Diffusion cieffiecient

$$D_{ij} = k\frac{T^{1.75}}{\rho\left(v_i^{1/3} + v_j^{1/3}\right)^2}\left[\frac{1}{M_i} + \frac{1}{M_j}\right]^{0.5} \quad (3)$$

Stefan Maxwell Effective Diffusion

$$D_{ij}^{eff} = D_{ij}\varepsilon^{1.5} \quad (4)$$

Total Molar Mass

$$M = \sum_{i=1}^{n} M_i\omega_i \quad (5)$$

Electrical Curret Density

$$M = \sum_{i=1}^{n} M_i\omega_i \quad (6)$$

Dij, binary diffusion coefficient for species i and j; k, Maxwell diffusion constant = 3.16x10-8 Pa·m2/s ; T, temperature = 353°K; υi, molar diffusion volume of j specie, cm3/mol; υO2 molar diffusion volume of O2 = 16.6x10-6 cm3/mol, υH2O molar diffusion volume of H2O = 12.7x10-6 cm3/mol, υN2 , molar diffusion volume of N2 = 17.9x10-6 cm3/mol; Mj, MO2, MH2O, and MN2, see Table I; ε, porosity = 0.5; ic, cathode current; Sa specific surface area = 1x107m2/m3; δ, active layer thickness = 10 um ; i0, exchange current density = 1.06x10-6 mA/cm2; F, Faraday's constant = 96485 C/mol, R, gas constant = 8.314 J/(mol·K); η, overpotential between 0.2-0.82 V; tH2O electro-osmotic drag = 3; gdl, gas diffusion layer thickness = 0.2 mm.

Five different air flow-field geometries adjacent to a PEMFC oxygen cathode were compared by numerical simulations.

The status conditions are shown in the following formulas:

Navier-Stokex, Normal velocity vector

$$u.n = u_0 . \quad (7)$$

Navier-Stokex, Outlet Pressure

$$p = p_0 \quad (8)$$

Navier Stokes, Velocity next the wall

$$u = 0 \quad (9)$$

Stefan.Maxwell, Convectibe flux

$$n_i.n = (\rho\omega_i u).n \quad (10)$$

Stefan Maxwell, velocity in pore

$$u = \frac{-n_{N2}}{\rho\omega_{N2}} \tag{11}$$

Electrochemical Reaction oxygen

$$n_{02}.n = M_{02}\frac{i_c}{4F} \tag{12}$$

Electromechanical Reaction water

$$n_{H_2O}.n = -M_{H_2O}\frac{i_c}{F}\left(\frac{1}{2}+t_{H_2O}\right) \tag{13}$$

The equiations *7, 8,9,10,11,12,13*, details the dimensions of the flow channels, and Fig. 1 shows the geometries of Designs 1 to 5. Design 1 consists of serpentine channels with abrupt changes in flow direction, while in Design 2, the direction of the flow was changed gradually. Figs. 1A and 1B present two versions of the serpentine flow-field design. The electrical current distributions of Designs 1 and 2 were compared, and the best one was chosen.

The dimensions of the selected design were then modified (Design 3), and once more the performances of the new flow-field geometry were compared with the other designs. See Fig. 1C.

Design 4 was based on continually re-directing the flow in a criss-cross pattern (3), and it is shown in Fig. 1D. The air flow was introduced via three intakes, each one equidistant from one another. Design 4 has been developed after a series of design iterations, each one providing a major leap in performance over the previous one. On the other hand, Design 5 used fifteen multiple parallel and straight channels (Fig. 1E), and each channel was fed with air at a constant pressure.

In this design the air flow was introduced via an intake located at the center of each group of five channels.

Parameter	Design 1 Dimensions	Design 2 Dimensions
Channel width	1 mm	1 mm
Channel depth	1 mm	1 mm
Rib width	1 mm	1 mm
Diffusion layer geometric area	12.32 cm^2	12.32 cm^2
Diffusion layer thickness	0.2 mm	0.2 mm
Geometric area for fluid flow	6.16 cm^2	5.97 cm^2
Flow/Mechanical-support relation**	50% /50%	52% /58%

Parameter	Design 3 Dimensions	Design 4 Dimensions	Design 5 Dimensions
Channel width	1 mm	1 mm	1 mm
Channel depth	1 mm	1 mm	1 mm
Rib width	1 mm	1x8x1 mm	1 mm
Diffusion layer geometric area	31.8 cm^2	31.8 cm^2	31.8 cm^2
Carbon cloth thickness	0.2 mm	0.2 mm	0.2 mm
Geometric area for fluid flow	15.19 cm^2	16.27 cm^2	15.9 cm^2
Channel length	152.73 cm	---------	12.6 cm
Flow/Mechanical support relation**	53%/47%	49%/51%	42%/58%

Table 1 Dimensions of the Designs used for this study

n, mass flux vector mol/s; u0, inlet velocity = 50 cc/min or 200cc/min, p0, outlet pressure = 1.013x105 Pa

This is the ratio between open area (OA) or area of the channel and the area of rib (AR). AR is the area of Mechanical-support.

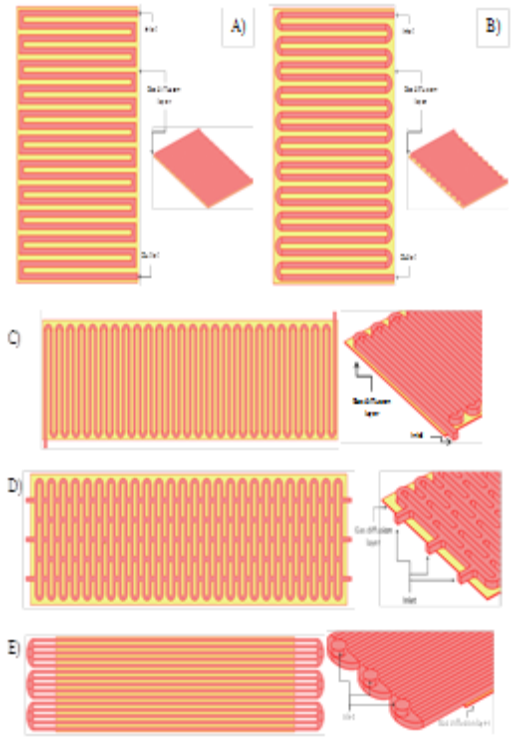

Figure 1 Design 1 consisted of serpentine channels with abrupt changes in flow direction. B) Design 2 consisted of serpentine channel with a more gradual change in flow direction; C) Design 3 (serpentine) consisted of curvilinear bends; D) Design 4 consisted in criss-cross pattern; and E) Design 5 was made with straight and parallel channels.

Results

Fig. 2 shows the measured gas velocity in Designs 1 and 2. A very slow flow velocity appears at the square corners when the flow changes direction abruptly (Fig. 2A). Therefore, water could accumulate here, which would lead to uneven gas and current distributions. A very slow flow-velocity region was not observed when the flow direction changed gradually (Design 2 in Fig. 2B).

Figs. 2C and 2D present the electrical current distributions in both designs at high cathode overpotential (0.8V). The porous media mitigate the effect of the slow flow-velocity regions, and the distributions of the current density were similar in both geometries. From computed polarization curves (which are not shown here for the sake of brevity) it was found that at low and medium power demands, both flow-field designs gave basically the same performance. At the higher power demand the performances differed but only slightly.

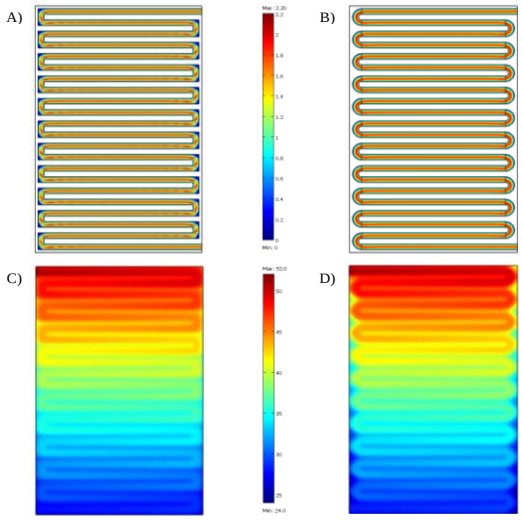

Figure 2 Flow velocity within the channels (m/s) in A) Design 1 and B) Design 2. Air introduced via an intake located at the top right side (inlet). The Electrical Current Density distribution obtained on the bottom of porous cathode for the C) Design 1 and D) Design 2. In this case the air introduced via an intake located at the top left side (inlet).

Fig. 3 shows the electrical current variation in the *y* axis, which is perpendicular to the downstream channel direction (Table II). The wave shape of the current variation was correlated with the lengths of both the channel and the rib (8). This Fig. shows that the electrical current decreased gradually along the *y* axis with the maximum value near the inlet. For example, when the distance was 4.4 cm the total electrical current at 0.8 V was 27.28 mA in Design 1 and 27.69 mA in Design 2.

ISSN-2410-3993

The difference in the total electrical currents between the two designs was 1.48%. Although this is a negligible difference between designs in one cell, this translates into a large difference in a stack configuration.

A comparison between these designs in terms of pressure drop with increasing Reynolds number was made by Boddu et al. (9). According to this author the serpentine square bends (Design 1) exhibit consistently higher pressure drops compared to the curvilinear bends used in Design 2. A large pressure drop leads to inefficient fuel cell performance. Also, because of fuel starvation is more likely to occur in Design 1, Design 2 was selected as the superior standard. Design 2 was therefore modified to create Design 3; see Figure 1C.

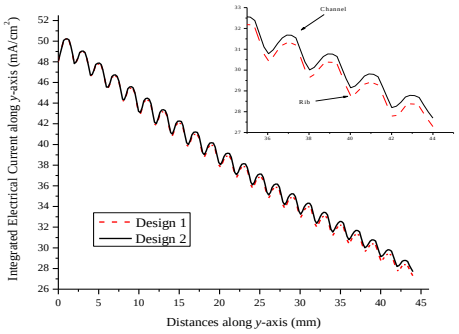

Figure 3 The Integrated Electrical Current along the y-axis, where the initial point of trajectory was located in the middle of the flow field (x=3.08 cm). Current density obtained in Designs 1 (- - -) and 2 (___) at cathode overpotential of 0.8 V.

The oxygen mass fraction distributions for Designs 3 to 5 are shown in Fig. 4. These appear to be more uniform in Designs 4 or 5 than in Designs 3. At a cathode overpotential of 0.66 V the final oxygen mass fraction in the gas diffusion layer was slightly lower than 0.123 in Design 3. In contrast, in Designs 4 and 5 the final oxygen mass fractions were slightly over 0.137. Again, this small difference observed in a single cell, can be significant in a stack configuration.

Fig. 5 shows the current density distributions for Designs 3 to 5 under a cell voltage of 0.52 V (i.e., cathode overpotential 0.66 V). The highest current density was obtained at the inlet where oxygen concentration was the highest. Fig. 5 clearly shows that the electrical current density in the outlet is lower in Design 3, and consequently a less efficient cell performance will be expected. In other words, Designs 4 and 5 produce more uniform electrical current density distributions over the porous cathode than Design 3. Consequently, Designs 4 and 5 can deliver superior performances.

At low electrical demands the performance of all fuel cells is governed by the electrode kinetics (equation [6]). In this case, the differences among gas-distribution designs are minimal, and those results are not shown for the sake of brevity. However, at medium electrical demands (Table V), the mass transport cannot keep up with the moderately fast kinetics, and the performance of Design 3 became mass-transport-limited. At higher electrical demands the performance of Design 3 deteriorates further (Table V). For example, at an overpotential of 0.82 V, the total current (1811mA) was significantly smaller than the total electrical current for Design 5 (2127 mA).

Design	50cc/min	200cc/min	200cc/min	200cc/min
	0.66 V	0.22 V	**0.52 V**	0.82 V
3	160.2	0.125	17.33	1811
4	168.4	0.125	17.35	2092
5	168.7	0.125	17.35	2127

Table 2 Total Current for different Desings at various operating conditions (m.A)

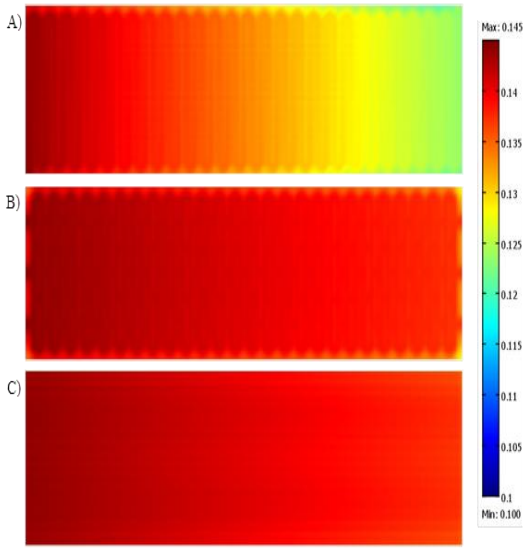

Figure 4 Mass Oxygen fraction. A) Design 3 (serpentine with curvilinear bends); B) Design 4 (criss-cross); and C) Design 5 (straight and parallel channels).

The re-direct pattern was conceived to provide a more uniform pressure field, thus resulting in a more constant gas flow distribution (10). Rivas (3) showed that the profiles of current density exhibit better distributions with the re-direct pattern design, to produce a more efficient fuel cell. Our results are in agreement with those presented by this author. On the other hand, Ferng (11) and Rivas (3) observed poor current distributions with parallel flow fields. The very slow gas flow velocities cause oxygen-starved areas in the gas diffusion layer. In design 5 the intakes were located efficiently in the current collectors, and therefore, more homogeneous current distributions were obtained. Incidentally, the difference between Designs 4 and 5 was rather small. This means that designs with intakes effectively located are very good alternatives from the performance standpoint. In addition, the small difference in total electrical current between designs 4 and 5 can be important in a stack configuration. Therefore, Design 5 is recommend for a stack configuration, see table V.

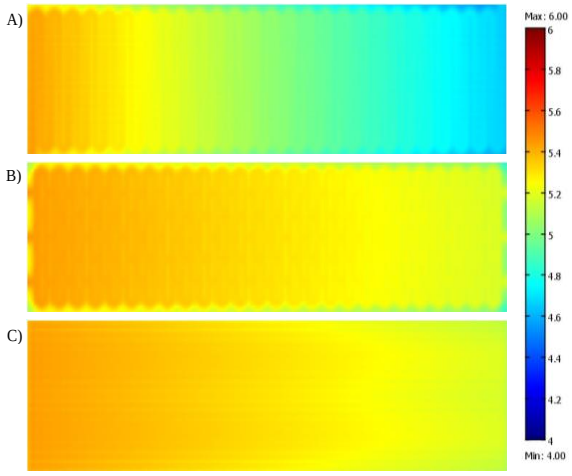

Figure 5 Electrical current distributions (mA/cm2) at the cathode (overpotential 0.66 V).. A) Design 3 (serpentine with curvilinear bends); B) Design 4 (criss-cross); and C) Design 5 (straight and parallel channels).

Conclusions

Five designs with different channel shapes and gas flow patterns were simulated numerically using Computational Fluid Dynamics (CFD). Using this approach, it was possible to conceive, detail, and analyze each design.

The electrical current distributions of the two different serpentine channels with square or rounded flow bends were tested. At higher loads the serpentine channels with abrupt changes in flow direction (Design 1) exhibit slightly lower electrical current distributions compared to curvilinear bends (Design 2). This minute difference within single cells across designs can have a large effect in a stack configuration. We recommend that the serpentine channel configuration should consist of curvilinear bends. Because of its better performance, Design 2 was selected for the second part of this investigation.

ISSN-2410-3993

The dimensions of the serpentine channel design with curvilinear bends were then modified (Design 3). Afterwards, Design 3 was compared to criss-cross (Design 4) and straight parallel channels (Design 5). The results showed that Designs 4 and 5 produce more uniform electrical current distributions than Design 3. This can be explained because the intakes were efficiently located. Therefore, we concluded that the effective placement of the intakes is as important as the shape of channel configuration.

Finally, the parallel channel flow field (Design 5) is the best alternative for current collectors due to its superior performance.

Acknowledgments

The authors thank the financial assistance provided by CONACYT (CB-2008-01-102018). Author P. E. Hidalgo also acknowledges CONACYT for scholarship support. Tech University of San Juan del Rìo, and CIDTEQ.

References

Ab, C. (2008). *Comsol multiphysics user's guide*. COMSOL AB: Burlington, MA.

Barreras, F., Lozano, A., Valiño, L., Mustata, R., & Marín, C. (2008). Fluid dynamics performance of different bipolar plates: Part I. Velocity and pressure fields. *Journal of Power Sources*, 175(2), 841-850.

Boddu, R., Marupakula, U. K., Summers, B., & Majumdar, P. (2009). Development of bipolar plates with different flow channel configurations for fuel cells. Journal of Power Sources, 189(2), 1083-1092.

Li, X., & Sabir, I. (2005). Review of bipolar plates in PEM fuel cells: Flow-field designs. International Journal of Hydrogen Energy, 30(4), 359-371.

Ferng, Y. M., Su, A., & Lu, S. M. (2008). Experiment and simulation investigations for effects of flow channel patterns on the PEMFC performance. International Journal of Energy Research, 32(1), 12-23.

Guzman, C., Verde, Y., Bustos, E., Manriquez, F., Terol, I., Arriaga, L. G., & Orozco, G. (2009). Preparation of Particulate Fuel Cell Electrodes by Electrodeposition Method. ECS transactions, 20(1), 413-423.

Park, J., & Li, X. (2007). An experimental and numerical investigation on the cross flow through gas diffusion layer in a PEM fuel cell with a serpentine flow channel. Journal of Power Sources, 163(2), 853-863.

Jeon, D. H., Greenway, S., Shimpalee, S., & Van Zee, J. W. (2008). The effect of serpentine flow-field designs on PEM fuel cell performance. International journal of hydrogen energy, 33(3), 1052-1066.

Lozano, A., Valiño, L., Barreras, F., & Mustata, R. (2008). Fluid dynamics performance of different bipolar plates: Part II. Flow through the diffusion layer. Journal of Power sources, 179(2), 711-722.

Perry R. H.,& Green D. W, (2008). Perry's Chemical Engineers´ Handbook, , 27th edition, McGraw-Hill, New York, p. 2-370

Rivas, S. V., Hidalgo, P. E., Chapman, T. W., & Orozco, G. (2010). Fluid Dynamics Study to Compare Two Different Flow-Field Geometries. ECS Transactions, 29(1), 195-204.